

1 Potential underestimation of ambient brown carbon absorption
2 based on the methanol extraction method and its impacts on
3 source analysis

4
5 Zhenqi Xu^a, Wei Feng^a, Yicheng Wang^a, Haoran Ye^a, Yuhang Wang^b, Hong Liao^a,
6 Mingjie Xie^{a,*}

7
8 ^aCollaborative Innovation Center of Atmospheric Environment and Equipment
9 Technology, Jiangsu Key Laboratory of Atmospheric Environment Monitoring and
10 Pollution Control, School of Environmental Science and Engineering, Nanjing
11 University of Information Science & Technology, 219 Ningliu Road, Nanjing 210044,
12 China

13 ^bSchool of Earth and Atmospheric Sciences, Georgia Institute of Technology, Atlanta,
14 GA 30332, United States

15
16 *Corresponding to:

17 Mingjie Xie (mingjie.xie@nuist.edu.cn, mingjie.xie@colorado.edu);

18 Mailing address: 219 Ningliu Road, Nanjing, Jiangsu, 210044, China

28 **Abstract**

29 The methanol extraction method was widely applied to isolate organic carbon (OC)
30 from ambient aerosols, followed by measurements of brown carbon (BrC) absorption.
31 However, undissolved OC fractions will lead to underestimated BrC absorption. In this
32 work, water, methanol (MeOH), MeOH/dichloromethane (MeOH/DCM, 1:1, v/v),
33 MeOH/DCM (1:2, v/v), tetrahydrofuran (THF), and N,N-dimethylformamide (DMF)
34 were tested for extraction efficiencies of ambient OC, and the light absorption of
35 individual solvent extracts was determined. Among the five solvents and solvent
36 mixtures, DMF dissolved the highest fractions of ambient OC (up to ~95%), followed
37 by MeOH and MeOH/DCM mixtures (< 90%), and the DMF extracts had significant
38 ($p < 0.05$) higher light absorption than other solvent extracts. This is because the OC
39 fractions evaporating at higher temperatures ($> 280^{\circ}\text{C}$) are less soluble in MeOH (~80%)
40 than in DMF (~90%) and contain stronger light-absorbing chromophores. Moreover,
41 the light absorption of DMF and MeOH extracts of collocated aerosol samples in
42 Nanjing showed consistent temporal variations in winter when biomass burning
43 dominated BrC absorption. While the average light absorption of DMF extracts was
44 more than two times greater than the MeOH extracts in late spring and summer. The
45 average light absorption coefficient at 365 nm of DMF extracts was 30.7% higher ($p <$
46 0.01) than that of MeOH extracts. Source apportionment results indicated that the
47 MeOH solubility of BrC associated with biomass burning, lubricating oil combustion,
48 and coal combustion is similar to their DMF solubility. The BrC linked with unburned
49 fossil fuels and polymerization processes of aerosol organics was less soluble in MeOH
50 than in DMF, which was likely the main reason for the large difference in time series
51 between MeOH and DMF extract absorption. These results highlight the importance of
52 testing different solvents to investigate the structures and light absorption of BrC,

53 particularly for the low-volatility fraction potentially originating from non-combustion
54 sources.

55

56

57

58

59

60

61

62

63

64

65

66

67

68

69

70

71

72

73

74

75

76

77

78 **1 Introduction**

79 Besides black carbon (BC) and mineral dust, growing evidence shows that organic
80 carbon (OC) aerosols derived from various combustion sources (e.g., biofuel and fossil
81 fuel) and secondary processes (e.g., gas-phase oxidation, aqueous and in-cloud
82 processes) can absorb sunlight at short visible and UV wavelengths (Laskin et al., 2015;
83 Hems et al., 2021). The radiative forcing (RF) of the light-absorbing organic carbon,
84 also termed “brown carbon” (BrC), is not well quantified due to the lack of its emission
85 data, complex secondary formations, and large uncertainties in *in situ* BrC
86 measurements (Wang et al., 2014; Wang et al., 2018; Saleh, 2020). The imaginary part
87 of the refractive index (k) of BrC is required when modeling its influence on aerosols
88 direct RF, and is retrieved by the optical closure method combining online monitoring of
89 aerosol absorption and size distributions with Mie theory calculations (Lack et al., 2012;
90 Saleh et al., 2013; Saleh et al., 2014). However, several pre-assumptions must be made
91 on aerosol morphology (spherical Mie model) and mixing states of BC and organic
92 aerosols (OA), which might introduce large uncertainties in the estimation of k (Mack
93 et al., 2010; Xu et al., 2021).

94 To improve the understanding on chemical composition and light-absorbing
95 properties of BrC chromophores, organic matter (OM) in aerosols was isolated through
96 solvent extraction using water and/or methanol, followed by filtration and a series of
97 instrumental analysis (e.g., UV/Vis spectrometer, liquid chromatograph-mass
98 spectrometer; Chen and Bond, 2010; Liu et al., 2013; Lin et al., 2016). Referring to
99 existing studies, a larger fraction of the methanol extract absorption comes from water-
100 insoluble OM containing conjugated structures (Chen and Bond, 2010; Huang et al.,
101 2020); the light absorption of biomass burning OM is majorly contributed by large
102 molecules (MW > 500~1000 Da; Di Lorenzo and Young, 2016; Di Lorenzo et al., 2017)

103 and depends on burn conditions (Saleh et al., 2014); polycyclic aromatic hydrocarbons
104 (PAHs) and nitroaromatic compounds (NACs) are ubiquitous BrC chromophores in the
105 atmosphere (Huang et al., 2018; Wang et al., 2019), but the identified species only
106 explain a few percentages (< 10%) of total BrC absorption (Huang et al., 2018; Li et
107 al., 2020).

108 Methanol can extract > 90% OM from biomass burning (Chen and Bond, 2010;
109 Xie et al., 2017b), while the extraction efficiency (η , %) decreases to ~80% for ambient
110 organic aerosols (Xie et al., 2019b; Xie et al., 2022) possibly due to other sources
111 emitting large hydrophobic molecules and oligomerizations of small molecules during
112 the aging process (Cheng et al., 2021; Li et al., 2021). The light-absorbing properties
113 and structures of methanol-insoluble OC (MIOC) are still unknown. By comparing BrC
114 characterization results of offline and online methods, some studies conclude that the
115 MIOC dominates BrC absorption in source and ambient aerosols (Bai et al., 2020; Atwi
116 et al., 2022). However, the online-retrieval and offline-extraction methods are designed
117 based on different instrumentation and purposes, and the online method depends largely
118 on presumed and uncertain optical properties of BC (Wang et al., 2014). Even when the
119 solvent extract absorption is converted to particulate absorption with Mie calculations,
120 pH and solvent matrix effects, as well as the potential incomplete solubility of BrC in
121 common solvents, should still be considered before comparing BrC absorption
122 measured directly in particles versus that derived from solvent extracts.~~Given that the~~
123 ~~solvent extract absorption is not converted to particulate absorption with Mie~~
124 ~~calculations, solvent and pH effects are not accounted for, and BrC is not completely~~
125 ~~dissolved in typical solvents (e.g., water and methanol), BrC absorption in particles and~~
126 ~~solution can hardly be compared directly.~~ To reveal the absorption and composition of
127 MIOC, it is necessary to find a new solvent or develop a new methodology to improve

128 OC extraction efficiency (Shetty et al., 2019).

129 In this work, a series of single solvents and solvent blends were tested for extraction
130 efficiencies of OC in ambient particulate matter with aerodynamic diameter $< 2.5 \mu\text{m}$
131 ($\text{PM}_{2.5}$), and the sample extract absorption of each solvent was compared. The solvent
132 or solvent mixture with the highest η value was applied to extract a matrix of collocated
133 $\text{PM}_{2.5}$ samples followed by light absorption measurements. In our previous work, the
134 light absorption of methanol extracts of the same samples was measured, and source
135 apportionment was performed using organic molecular marker data (Xie et al., 2022).
136 By comparing with the study results in Xie et al. (2022), this study evaluated potential
137 underestimation of BrC absorption in methanol and its impacts on BrC source
138 attributions. These results suggest that different solvents should be used in future
139 investigations on the absorption, composition, sources, and formation pathways of low-
140 volatility BrC.

141 **2. Methods**

142 *2.1 Solvent selection*

143 Five solvents and solvent mixtures including water, methanol (MeOH),
144 MeOH/dichloromethane (MeOH/DCM, 1:1, v:v), MeOH/DCM (1:2, v:v),
145 tetrahydrofuran (THF), and N,N-dimethylformamide (DMF) were selected to extract
146 OC from identical $\text{PM}_{2.5}$ samples to determine which solvent or solvent mixture has the
147 highest η value. Water and methanol are the most commonly used solvents to extract
148 BrC from source or ambient particles. Cheng et al. (2021) found that OC produced
149 through the combustion of toluene, isooctane, and cyclohexane were more soluble in
150 DCM than MeOH. Since a major part of BrC absorption is coming from unknown large
151 molecules (Di Lorenzo and Young, 2016; Di Lorenzo et al., 2017), polar aprotic
152 solvents THF and DMF were tested due to their high capacity for dissolving large

153 polymers. Except for water and MeOH, DCM and THF were rarely used to extract OC
154 for light absorption measurements (Cheng et al., 2021; Moschos et al. 2021), and DMF
155 has not ever been tested for extracting BrC in literature.

156 *2.2 Sampling*

157 **Sampling for solvent test.** To compare OC extraction efficiencies and extract
158 absorption of the five selected solvents and solvent mixtures, twenty-one ambient PM_{2.5}
159 samples were collected on the rooftop of a seven-story library building in Nanjing
160 University of Information Science and Technology (NUIST, 32.21°N, 118.71°E).
161 Details of the sampling site and equipment were provided by Yang et al. (2021). Two
162 identical mid-volume samplers (Sampler I and II; PM_{2.5}-PUF-300, Mingye
163 Environmental, China) equipped with 2.5 μm cut-point impactors were used for
164 ambient air sampling during day-time (8:00 a.m.–7:00 p.m.) and night-time (8:00 p.m.–
165 7:00 a.m. the next day), respectively, in December 2019. After the impactor, PM_{2.5} in
166 the air stream was collected on a pre-baked (550 °C, 4 h) quartz filter (20.3 cm ×12.6
167 cm, Munktell Filter AB, Sweden) at a flow rate of 300 L min⁻¹. PM_{2.5} filter and field
168 blank samples were sealed and stored at –20 °C before chemical analysis. Information
169 about PM_{2.5} samples for the solvent test is provided in Table S1 of supplementary
170 information.

171 **Ambient sampling for BrC analysis.** Details of the ambient sampling were described
172 in previous work (Qin et al., 2021; Yang et al., 2021; Xie et al., 2022). Briefly, Sampler
173 I and II were equipped with two quartz filters in series (quartz behind quartz, QBQ
174 method; Q_f and Q_b) followed by adsorbents. Collocated filter and adsorbent samples
175 were collected every sixth day during daytime and nighttime from 2018/09/28 to
176 2019/09/28. Field blank sampling was performed every 10th sample to address
177 contamination. Q_f samples loaded with PM_{2.5} were speciated and extracted for light

178 absorption measurements. The OC adsorbed on Q_b and its light absorption were
179 analyzed to determine positive sampling artifacts. The adsorbents in sampler I [a
180 polyurethane foam (PUF)/XAD-4 resin/PUF sandwich] and II (a PUF plug) were used
181 to collect gas-phase nonpolar and polar organic compounds, respectively. The
182 measurement results of gas- and particle-phase organic compounds were provided by
183 Gou et al. (2021) and Qin et al. (2021).

184 *2.3 Solvent test for light absorption and extraction efficiency*

185 An aliquot ($\sim 6 \text{ cm}^2$) of each filter sample was extracted ultrasonically in 10 mL of
186 each solvent or solvent mixture (HPLC grade) for 30 min (one-time extraction
187 procedure, $N = 11$; Table S1). After filtration, the light absorbance (A_λ) of individual
188 solvent extracts was measured over 200–900 nm using a UV/Vis spectrometer (UV-
189 1900, Shimadzu Corporation, Japan), and was converted to light absorption coefficient
190 ($\text{Abs}_\lambda, \text{Mm}^{-1}$) by

$$191 \text{Abs}_\lambda = (A_\lambda - A_{700}) \times \frac{V_l}{V_a \times L} \ln(10) \quad (1)$$

192 where A_{700} is subtracted to correct baseline drift, V_l (m^3) is the air volume of the
193 extracted sample, L (0.01 m) is the optical path length, and $\ln(10)$ was multiplied to
194 transform Abs_λ from a common to a natural logarithm (Hecobian et al., 2010). To
195 understand if multiple extractions could draw out more BrC, a two-time extraction
196 procedure was applied for another 10 ambient $\text{PM}_{2.5}$ samples in the same manner (Table
197 S1). The A_λ of the 1st and 2nd extractions (10 mL each) was measured separately for
198 Abs_λ calculations.

199 Prior to solvent extractions, the concentrations of OC and EC in each filter sample
200 were analyzed using a thermal-optical carbon analyzer (DRI, 2001A, Atmoslytic,
201 United States) following the IMPROVE-A protocol. OC and EC were converted to CO_2

202 step by step during two separate heating cycles [OC1 (140°C) – OC2 (280°C) – OC3
203 (480°C) – OC4 (580°C) in pure He, EC1 (580°C) – EC2 (740°C) – EC3 (840°C) in 98%
204 He/2% O₂], and the emitted CO₂ during each heating step was converted to CH₄ and
205 measured using a flame ionization detector (FID).

206 After extractions, filters extracted by MeOH, MeOH/DCM (1:1), MeOH/DCM
207 (1:2), and THF were air-dried in a fume hood and analyzed for residual OC (rOC, μg
208 m⁻³) using the identical method. Filters extracted in water and DMF cannot be air-dried
209 in the short term due to the low volatility of solvents, and their rOC was measured after
210 baking at 100 °C for 2 h. The total amount of OC dissolved in water for each sample
211 was also measured as water-soluble OC (WSOC) by a total organic carbon analyzer
212 (TOC-L, Shimadzu, Japan; Yang et al., 2021). To examine if the baking process would
213 influence rOC measurements, the rOC of filters extracted in MeOH, MeOH/DCM
214 mixtures, and THF were also measured after the baking process and compared to those
215 determined after air dried. The pyrolytic carbon (PC) was used to correct for sample
216 charring and was determined when the filter transmittance or reflectance returned to its
217 initial value during the analysis (Schauer et al., 2003), but the formation of PC is very
218 scarce when analyzing extracted filters. In this study, solvent-extractable OC (SEOC,
219 μg m⁻³) was determined by the difference in OC1–OC4 between pre- and post-
220 extraction samples. The extraction efficiency (η, %) of each solvent was expressed as

$$221 \quad \eta = \frac{\text{SEOC}}{\text{OC}} \times 100\% \quad (2)$$

222 Here, SEOC denotes WSOC when the solvent is water. For the ambient samples
223 extracted twice, rOC was measured only after the two-extraction procedure was
224 completed.

225 The solution mass absorption efficiency (MAE_λ, m² g⁻¹ C) was calculated by
226 dividing Abs_λ by the concentration of SEOC

227 $MAE_{\lambda} = \frac{Abs_{\lambda}}{SEOC}$ (3)

228 and the solution absorption Ångström exponent (\AA), a parameter showing the
 229 wavelength dependence of solvent extract absorption, was obtained from the regression
 230 slope of $\lg(Abs_{\lambda})$ versus $\lg(\lambda)$ over 300–550 nm.

231 The solvent effect is not uncommon when measuring aerosol extract absorbance in
 232 different solvents (Chen and Bond, 2010; Mo et al., 2017; Moschos et al., 2021), but
 233 is rarely accounted for in previous studies. To evaluate the influence of solvent effects
 234 on light absorption of different solvent extracts of the same sample, solutions of 4-
 235 nitrophenol at 1.90 mg L^{-1} , 4-nitrocatechol at 1.84 mg L^{-1} , and 25-PAH mixtures (Table
 236 S2) at 0.0080 mg L^{-1} and 0.024 mg L^{-1} (each species) in the five solvents and solvent
 237 mixtures were made up for five times and analyzed for UV/Vis spectra. The absorbance
 238 of PAH mixtures in water was not provided due to their low solubility.

239 *2.3 Measurements and analysis of ambient BrC absorption*

240 Collocated Q_f and Q_b samples were extracted using the solvent with the highest η
 241 value once followed by light absorbance measurement. OC concentrations in Q_f and Q_b
 242 samples were obtained from Yang et al. (2021), and SEOC values were estimated from
 243 OC concentrations and the average η value determined in *section 2.1* for one-time
 244 extraction. In this work, Q_b measurements were used to correct Abs_{λ} , MAE_{λ} , and \AA of
 245 BrC in ambient $PM_{2.5}$ in the same manner as those for water and methanol extracts in
 246 Xie et al. (2022)

247 Artifact-corrected $Abs_{\lambda} = Abs_{\lambda}^{Q_f} - Abs_{\lambda}^{Q_b}$ (4)

248 Artifact-corrected $MAE_{\lambda} = \frac{Abs_{\lambda}^{Q_f} - Abs_{\lambda}^{Q_b}}{SEOC_{Q_f} - OC_{Q_b}}$ (5)

249 where $Abs_{\lambda}^{Q_f}$ and $Abs_{\lambda}^{Q_b}$ are Abs_{λ} values of Q_f and Q_b samples, respectively; $SEOC_{Q_f}$
 250 represents SEOC concentrations in Q_f samples; OC_{Q_b} denotes OC concentrations in Q_b

251 samples, assuming that OC in Q_b is completely dissolved (Xie et al., 2022). Artifact
252 corrected \dot{A} were generated from the regression slope of $\lg(\text{Abs}^{Q_f}_\lambda - \text{Abs}^{Q_b}_\lambda)$ versus \lg
253 (λ) over 300 – 550 nm. Artifact-corrected Abs_λ , MAE_λ , and \dot{A} during each sampling
254 interval were determined by averaging each pair of collocated measurements. If one of
255 the two numbers in a pair is missed, the other number will be directly used for the
256 specific sampling interval. To compare with previous studies based on water and/or
257 methanol extraction methods, Abs_λ and MAE_λ at 365 nm were shown and discussed in
258 this work.

259 Pearson's correlation coefficient (r) was used to show how collocated
260 measurements of BrC in ambient $\text{PM}_{2.5}$ vary together. The coefficient of divergence
261 (COD) was calculated to indicate consistency between collocated measurements. The
262 relative uncertainty of BrC absorption derived from duplicate data was depicted using
263 the average relative percent difference (ARPD, %), which was used as the uncertainty
264 fraction for BrC measurements. Calculation methods of COD and ARPD are provided
265 in Text S1 of supplementary information. To examine the influence of potential BrC
266 underestimation based on the methanol extraction method on source apportionment,
267 positive matrix factorization (PMF) version 5.0 (U.S. Environmental Protection
268 Agency) was applied to attribute the light absorption of aerosol extracts in methanol
269 and solvent with the highest η to sources. The total concentration data ($Q_f + Q_b +$
270 adsorbent) of organic compounds have been used to apportion the light absorption of
271 MeOH-soluble OC to specific sources (Xie et al., 2022), so as to avoid the impacts of
272 gas-particle partitioning. In this work, the input particulate bulk components and total
273 organic molecular marker (OMM) data for PMF analysis were obtained from Xie et al.
274 (2022) and are summarized in Table S3. Four- to ten-factor solutions were tested to
275 retrieve a final factor number with the most physically interpretable base-case solution.

276 More information on input data preparation and the factor number determination are
277 provided in supplementary information (Text S2 and Table S4).

278 **3. Results and discussion**

279 *3.1 Solvent test*

280 3.1.1 Extraction efficiency of different solvents

281 The concentrations of OC and EC fractions in each sample prior to solvent
282 extractions are listed in Table S1. SEOC concentrations and extraction efficiencies of
283 individual solvents and solvent mixtures are detailed in Table 1. Generally, DMF
284 presented the highest extraction efficiency of total OC whenever filter samples were
285 extracted once ($89.0 \pm 7.96\%$) or twice ($95.6 \pm 3.67\%$), followed by MeOH (one-time
286 extraction $82.3 \pm 8.68\%$, two-time extraction $86.6 \pm 7.86\%$) and MeOH/DCM mixtures
287 ($\sim 75\%$, $\sim 85\%$). Although THF and DMF are frequently used to dissolve polymers (e.g.,
288 polystyrene) for characterization, THF had the lowest η values ($64.2 \pm 8.08\%$, $70.1 \pm$
289 8.01%) comparable to water ($66.7 \pm 8.58\%$, $69.9 \pm 5.88\%$). Compared with one-time
290 extraction, the extraction efficiencies of selected solvents were improved by a few
291 percent when filter samples were extracted twice, and η values of MeOH/DCM
292 mixtures became closer to those of MeOH (Table 1). These results showed that solvents
293 can reach more than 80% of their dissolving capacity with the one-time extraction, and
294 the ambient OC in Nanjing is more soluble in MeOH than in DCM.

295 From OC1 to OC4, the volatility of OC fractions is expected to decrease
296 continuously, and the molecules in OC fractions evolving at higher temperatures should
297 be larger than those in OC1 with similar functional groups. In Table 1, MeOH and
298 MeOH/DCM mixtures had comparable or even higher η values ($82.6 \pm 25.9\%$ – $97.9 \pm$
299 5.02%) of OC1 and OC2 than DMF ($88.8 \pm 4.98\%$ – $97.2 \pm 2.12\%$). But OC3 and OC4
300 accounted for more than 60% of OC concentrations, and DMF exhibited significant (p

301 < 0.05) larger η values than other solvents, indicating that DMF had stronger dissolving
302 capacity for large organic molecules than MeOH.

303 Concentrations of extracted OC fractions in MeOH, MeOH/DCM mixtures, and
304 THF based on the two methods for rOC measurements (*section 2.2*) are compared in
305 Figures S1 and S2. The total SEOC concentrations derived from the two methods are
306 compared in Figure S3. All the scatter data of SEOC fell along the 1:1 line with
307 significant correlations ($r > 0.85$, $p < 0.01$). Because the measurement uncertainty of
308 dominant species is lower than minor ones (Hyslop and White, 2008; Yang et al., 2021),
309 the slightly greater relative difference between the two methods for extractable OC1
310 was likely attributed to its low concentrations ($< 1 \mu\text{g m}^{-3}$; Tables 1 and S1). Thus,
311 baking extracted filters to dryness was expected to have little influence on SEOC
312 measurements, particularly for low-volatility OC fractions (OC2-OC4).

313 Although water dissolves less OC than MeOH, WSOC is intensively extracted and
314 analyzed for its composition and light absorption (Hecobian et al., 2010; Liu et al., 2013;
315 Washenfelder et al., 2015). WSOC can play a significant role in changing the radiative
316 and cloud-nucleating properties of atmospheric aerosols (Hallar et al., 2013; Taylor et
317 al., 2017). It also served as a proxy measurement for oxygenated (OOA) or secondary
318 organic aerosols (SOA) in some regions (Kondo et al., 2007; Weber et al., 2007). In
319 previous work, MeOH was commonly used as the most efficient solvent in extracting
320 OC from biomass burning ($\eta > 90\%$; Chen and Bond, 2010; Xie et al., 2017b) and
321 ambient particles ($\eta \sim 80\%$; Xie et al., 2019b; Xie et al., 2022). MeOH-insoluble OC
322 has rarely been investigated through direct solvent-extraction followed by instrumental
323 analysis. There is evidence showing that BrC absorption is associated mostly with large
324 molecular weight and extremely low-volatility species (Saleh et al., 2014; Di Lorenzo
325 and Young, 2016; Di Lorenzo et al., 2017). Compared with DMF, the lower capability

326 of MeOH in dissolving OC3 and OC4 would lead to an underestimation of BrC
327 absorption in atmospheric aerosols.

328 3.1.2 Light absorption of different solvent extracts

329 Table 2 shows the average Abs_{λ} and MAE_{λ} values of different solvent extracts at
330 365 and 550 nm. The Abs_{λ} and MAE_{λ} spectra of selected samples are illustrated in
331 Figure S4. Not including DMF, MeOH extracts exhibited the strongest light absorption.
332 Since MeOH can dissolve more OC3 and OC4 than DCM (Table 1), the Abs_{λ} and MAE_{λ}
333 of MeOH/DCM extracts decreased as the fraction of DCM increased in solvent
334 mixtures (Table 2 and Figure S4). Water and THF extracts had the smallest Abs_{λ} and
335 MAE_{λ} due to their low extraction efficiencies for low-volatility OC (OC2-OC4; Table
336 1). In comparison to MeOH extracts, $Abs_{365/550}$ and $MAE_{365/550}$ of DMF extracts were
337 at least more than 40% higher ($p < 0.05$). Given that the relative difference in extraction
338 efficiency of total OC between MeOH and DMF was less than 10% and DMF dissolved
339 more OC3 and OC4 than other solvents (Table 1), low-volatility OC should contain
340 stronger light-absorbing chromophores (Saleh et al., 2014) and its mass fraction might
341 determine the difference in BrC absorption across solvent extraction methods.
342 Moreover, the relative difference in Abs_{λ} and MAE_{λ} between MeOH and DMF extracts
343 increased with wavelength (Table 2 and Figure S4). This is because the light absorption
344 of DMF extracts that contain stronger BrC chromophores depends less on wavelengths
345 than other solvent extracts ($\text{\AA} \sim 4.5$, Table 2). As shown in Figure S5, average \AA and
346 $MAE_{365/550}$ values of individual solvent extracts in Table 2 are negatively correlated.

347 In this work, insoluble organic particles coming off the filter during sonication
348 might lead to overestimated SEOC concentrations and η values, and then the MAE_{λ} of
349 solvent extracts would be underestimated. Previous studies rarely considered the loss
350 of insoluble OC during the extraction process (Yan et al., 2020), of which the impact

351 on MAE_λ calculation was still inconclusive. But Abs_λ measurements would never be
352 influenced, as the light absorbance of solvent extracts was analyzed after filtration. In
353 Table 2, the second extraction only increases the average Abs₃₆₅ and Abs₅₅₀ values of
354 DMF extracts by 6.70% ($p = 0.78$) and 6.76% ($p = 0.77$), respectively. We suspected
355 that the difference in η values of DMF between one-time and two-time extraction
356 procedures was mainly ascribed to the detachment of insoluble OC particles.

357 In Figure S6, the absorbance spectra of 4-nitrophenol and 4-nitrocatechol in water
358 shift toward longer wavelengths compared to their MeOH solution. This is because
359 neutral and deprotonated forms of 4-nitrophenol and 4-nitrocatechol may have different
360 absorbance spectra, and these two compounds are deprotonated at $\text{pH} \approx 7$ (Lin et al.,
361 2015b, 2017). The strong light absorption of 4-nitrophenol and 4-nitrocatechol in DMF
362 at 450 nm was not observed in other solvents, and was likely caused by unknown
363 reactions. Then the solvent effect introduced by DMF might overestimate the light
364 absorption of low-molecular-weight (LMW) nitrophenol-like species at > 400 nm in
365 source or ambient aerosols. Evidence shows that BrC absorption is dominated by large
366 molecules with extremely low volatility (Saleh et al., 2014; Di Lorenzo and Young,
367 2016; Di Lorenzo et al., 2017), and LMW nitrophenol-like species have very low
368 contributions to particulate OM (e.g., $< 1\%$) and aerosol extract absorption (e.g., $< 10\%$)
369 (Mohr et al., 2013; Zhang et al., 2013; Teich et al., 2017; Xie et al., 2019a, 2020; Li et
370 al., 2020). The shapes of the light absorption spectra of aerosol extracts in DMF were
371 similar to other solvents (Figure S4) and PAH solutions (Figure S6g-l), and no elevation
372 in light absorption appeared at 400–500 nm. Thus, the overestimated absorption of
373 LMW nitrophenol-like species in DMF might not substantially impact the overall BrC
374 absorption of aerosol extracts. Furthermore, the absorbance of 4-nitrophenol and 4-
375 nitrocatechol in DMF at 365 nm (A_{365}) was lower than that in MeOH, and PAH

376 solutions showed very similar absorbance spectra across the five solvents (Figure S6g–
377 1 and Table S5). Considering that low-volatility OC fractions (e.g., OC3 and OC4) in
378 the ambient are less water soluble (Table 1) and have a high degree of conjugation
379 (Chen and Bond, 2010; Lin et al., 2014), their structures are probably featured by a
380 PAH skeleton. Therefore, the large difference in Abs_{365} between DMF and MeOH
381 extracts (Table 2) was primarily ascribed to the fact that DMF can dissolve more OC3
382 and OC4 than methanol (Table 1). However, we cannot rule out the impact of solvent
383 effects on the comparison of light absorption spectra between MeOH and DMF extracts
384 (Figure S4), and more work is warranted in identifying the structures more soluble in
385 DMF than in MeOH.

386 *3.2 Collocated measurements and temporal variability*

387 Abs_{365} values of collocated Q_f and Q_b extracts in DMF are summarized in Table S6.
388 No significant difference was observed (Q_f $p = 0.96$; Q_b $p = 0.42$) between the two
389 samplers. After Q_b corrections, Abs_{365} , MAE_{365} , and \dot{A} of DMF extractable OC ($Abs_{365,d}$,
390 $MAE_{365,d}$, and \dot{A}_d) in $PM_{2.5}$ were calculated by averaging each pair of duplicate Q_f – Q_b
391 data, and are compared with those of methanol extracts ($Abs_{365,m}$, $MAE_{365,m}$, and \dot{A}_m)
392 in Table 3. Figure 1 shows comparisons between collocated measurements of $Abs_{365,d}$,
393 $MAE_{365,d}$, and \dot{A}_d . Generally, all comparisons indicated good agreement with $COD <$
394 0.20 (0.094 – 0.15). $Abs_{365,d}$ and $MAE_{365,d}$ had comparable uncertainty fractions (ARPD,
395 22.7% and 24.5% , Figure 1) as $Abs_{365,m}$ and $MAE_{365,m}$ (28.4% and 28.8% ; Xie et al.,
396 2022). Since different primary combustion sources can have similar spectral
397 dependence for BrC absorption (Chen and Bond, 2010; Xie et al., 2017b; Xie et al.,
398 2018; Xie et al., 2019a), most \dot{A}_d data clustered on the identity line with much lower
399 variability than $Abs_{365,d}$ and $MAE_{365,d}$. As shown in Table 3, average $Abs_{365,d}$ and
400 $MAE_{365,d}$ values were 30.7% ($p < 0.01$) and 17.3% ($p < 0.05$) larger than average

401 $Abs_{365,m}$ and $MAE_{365,m}$. Because the k value of BrC in bulk solution is directly estimated
402 from Abs_{λ} or MAE_{λ} (Liu et al., 2013; Liu et al., 2016; Lu et al., 2015), the estimation
403 method needs to be revised when ambient BrC is extracted using DMF instead of
404 MeOH. Both $MAE_{365,d}$ and $MAE_{365,m}$ were negatively correlated ($p < 0.01$) with their
405 corresponding \dot{A} values (Figure S7), and the lower average \dot{A}_d (5.25 ± 0.64 , $p < 0.01$)
406 compared to \dot{A}_m (6.81 ± 1.64 ; Table 3) supports that more-absorbing BrC had less
407 spectral dependence than less-absorbing BrC.

408 Figure 2 compares the time series of Abs_{365} , MAE_{365} , and \dot{A} between the DMF and
409 MeOH extracts. Both DMF and MeOH extracts had significant ($p < 0.05$) higher
410 absorption at night-time than during the daytime due to the “photo-bleaching” effect
411 (Zhang et al., 2020; Xie et al., 2022). All the three parameters of DMF and MeOH
412 extracts exhibited consistency in winter (Figure 2) when biomass burning dominated
413 BrC absorption (Xie et al., 2022). While in later spring and summer (2019/05/15–
414 2019/08/01), average $Abs_{365,d}$ and $MAE_{365,d}$ values were more than two times greater
415 than the average $Abs_{365,m}$ and $MAE_{365,m}$. Many studies have identified a temporal
416 pattern of BrC absorption with winter maxima and summer minima based on
417 water/MeOH extraction methods (Lukács et al., 2007; Zhang et al., 2010; Du et al.,
418 2014; Zhu et al., 2018). Due to the low capability of water and MeOH in dissolving
419 large BrC molecules, BrC absorption and its temporal variations in these studies might
420 be biased. Moreover, the identification of BrC sources using receptor models is highly
421 dependent on the difference in the time series of input species (Dall'Osto et al., 2013).
422 Then, using DMF instead of MeOH for BrC extraction and measurements will lead to
423 distinct source apportionment results.

424 3.3 Sources of DMF and MeOH Extractable BrC

425 A final factor number of eight was determined based on the interpretability of

426 different base-case solutions (four to ten factors), the change in Q/Q_{exp} with factor
427 numbers, and robustness analysis (Text S2 and Table S4). Normalized factor profiles of
428 seven- to nine-factor solutions are compared in Figure S8. The seven-factor solution
429 failed to resolve the lubricating oil combustion factor characterized by hopanes and
430 steranes (Figure S8c). An unknown factor containing various source tracers related to
431 crustal dust (Ca^{2+} and Mg^{2+}), lubricating oil (hopanes and steranes), and soil microbiota
432 (sugar and sugar alcohols) was identified in the nine-factor solution (Figure S8i).
433 Median and mean values of input $\text{Abs}_{365,\text{d}}$, $\text{Abs}_{365,\text{m}}$, and bulk component concentrations
434 agreed well with PMF estimations (Table S7), and the strong correlations ($r = 0.86$ –
435 0.99) between observations and PMF estimations indicated that the eight-factor
436 solution simulated the time series of input species well. In comparison to Xie et al.
437 (2022), where Abs_{365} of MeOH and water extracts were apportioned to nine sources
438 using the same speciation data, this work lumped secondary nitrate and sulfate to the
439 same factor (termed “secondary inorganics”, Figure S8h), and the other seven factors
440 had similar factor profiles linked with biomass burning, non-combustion fossil,
441 lubricating oil combustion, coal combustion, dust resuspension, biogenic emission, and
442 isoprene oxidation. Interpretations of individual factors based on characteristic source
443 tracers and contribution time series were provided in previous work (Gou et al., 2021;
444 Xie et al., 2022).

445 The average relative contributions of the identified factors to $\text{Abs}_{365,\text{d}}$, $\text{Abs}_{365,\text{m}}$, and
446 bulk components are listed in Table S8. Consistent contribution distributions of $\text{Abs}_{365,\text{m}}$
447 were observed between Xie et al. (2022) and this study, indicating that the PMF results
448 were robust to the inclusion of $\text{Abs}_{365,\text{d}}$ data. Figure 3 compares the time series of factor
449 contributions to $\text{Abs}_{365,\text{d}}$ and $\text{Abs}_{365,\text{m}}$. ARPD and COD values between factor
450 contributions to $\text{Abs}_{365,\text{d}}$ and $\text{Abs}_{365,\text{m}}$ and the absolute difference are exhibited in Figure

451 S9. Abs_{365,d} and Abs_{365,m} had comparable contributions from biomass burning,
452 lubricating oil combustion, and coal combustion (Figure 3a, c, d). The small COD
453 values of these three factors (0.0041–0.17) indicated no significant divergence. The
454 biogenic emission and isoprene oxidation factors exhibited complete difference (ARPD
455 = 200%, COD = 1; Figure S9f, g) as they had no contribution to Abs_{365,m}. Among the
456 eight factors, the non-combustion fossil, dust resuspension, and isoprene oxidation
457 factors had the largest median difference in factor contributions to Abs_{365,d} and Abs_{365,m}
458 (0.63–0.67 Mm⁻¹) with substantial heterogeneity (COD > 0.20), followed by the
459 secondary inorganics factor (0.20 Mm⁻¹, COD = 0.41). The temporal variations of the
460 absolute difference shown in Figure S9 are identical to the contributions of individual
461 factors to Abs_{365,d} or Abs_{365,m} (Figure 3).

462 The non-combustion fossil factor represents unburned fossil-fuel emissions (e.g.,
463 petroleum products), which contain substantial large organic molecules (e.g., high MW
464 PAHs; Simoneit and Fetzer, 1996; Mi et al., 2000). This might explain why the non-
465 combustion fossil factor contributed more Abs_{365,d} than Abs_{365,m} all over the year
466 (Figure S9b). Dust resuspension and isoprene oxidation factors show prominent
467 contributions to Abs_{365,d} in spring and summer, respectively (Figure 3e, g). The dust
468 resuspension factor had the highest average contributions to both crustal materials (Ca²⁺
469 and Mg²⁺) and carbonaceous species (OC and EC; Table S8 and Figure S8), and was
470 considered a mixed source of crustal dust and motor vehicle emissions (Yu et al., 2020;
471 Xie et al., 2022). Besides the influences from primary emissions, aging processes of
472 organic components in dust aerosols can induce the formation of BrC through iron-
473 catalyzed polymerization (Link et al., 2020; Al-Abadleh, 2021; Chin et al., 2021). It
474 was demonstrated that the isoprene-derived polymerization products through aerosol-
475 phase reactions are light-absorbing chromophores (Lin et al., 2014; Nakayama et al.,

476 2015). This might explain the elevated difference between Abs_{365,d} and Abs_{365,m}
477 contributions of the isoprene oxidation factor in summer (Figure S9g). The biogenic
478 emission factor was characterized by tracers related to microbiota activities (sugar and
479 sugar alcohols) and decomposition of high plant materials (odd-numbered alkanes) in
480 soil (Rogge et al., 1993; Simoneit et al., 2004), and had negligible contributions (<0.1%)
481 to Abs_{365,d} and Abs_{365,m}. Evidence shows that secondary BrC can be generated through
482 gas-phase reactions of anthropogenic volatile organic compounds with NO_x
483 (Nakayama et al., 2010; Liu et al., 2016; Xie et al., 2017a), aqueous reactions of SOA
484 with reduced nitrogen-containing species (e.g., NH₄⁺; Updyke et al., 2012; Powelson et
485 al., 2014; Lin et al., 2015a), and evaporation of water from droplets in the atmosphere
486 containing soluble organics (Nguyen et al., 2012; Kasthuriarachchi et al., 2020). These
487 processes can also lead to the formation of low-volatility oligomers (Nguyen et al.,
488 2012; Song et al., 2013), and their contributions might be lumped into the secondary
489 inorganics factor due to the lack of OMMs. According to these results, one possible
490 explanation for the difference in time series between Abs_{365,d} and Abs_{365,m} (Figure 2) is
491 that large BrC molecules from unburned fossil fuels and atmospheric processes are less
492 soluble in MeOH than in DMF.

493 **4. Conclusions and implications**

494 Comparisons of extraction efficiencies and light absorption of ambient aerosol
495 extracts across selected solvents and solvent mixtures indicate that MeOH may
496 sometimes be replaced with DMF for measuring BrC absorption, as low-volatility OC
497 fractions containing strong chromophores are less soluble in MeOH than in DMF.
498 Existing modeling studies on the radiative forcing of BrC (Feng et al., 2013; Wang et
499 al., 2014; Zhang et al., 2020) often retrieved or estimated its optical properties from
500 laboratory or ambient measurements based on water/methanol extraction methods

501 (Chen and Bond, 2010; Hecobian et al., 2010; Liu et al., 2013; Zhang et al., 2013), and
502 had a potential to underestimate the contribution of BrC to total aerosol absorption.
503 However, the influence of the solvent effect was not accounted for in this work when
504 comparing the light absorption of different solvent extracts. The difference between
505 MeOH and DMF extract absorption might change with the time and location due to the
506 variations in BrC sources. The results of this work also imply the necessity of applying
507 different solvents or combinations of solvents with broad polarity and dissolving
508 capability to study BrC composition and absorption, particularly for low-volatility
509 fractions.

510 Although light-absorbing properties of DMF and MeOH extracts had good
511 agreement in cold periods, when biomass and coal burning sources dominated BrC
512 emissions, their distinct time series in spring and summer implies that the contributions
513 of certain BrC sources were underestimated or missed when the MeOH extraction
514 method was used. Source apportionment results of $Abs_{365,d}$ and $Abs_{365,m}$ based on
515 organic molecular marker data indicated that large and methanol insoluble BrC
516 molecules are likely coming from unburned fossil fuels and polymerization of aerosol
517 organics. Laboratory studies have observed the polymerization process through
518 heterogeneous reactions of several precursors (e.g., catechol; Lin et al., 2014; Link et
519 al., 2020), but the structures and light-absorbing properties of potential polymerization
520 products in ambient aerosols (Figure 3e, g) are less understood and warrant further
521 study.

522

523 ***Data availability***

524 Data used in the writing of this paper is available at the Harvard Dataverse
525 (<https://doi.org/10.7910/DVN/CGHPXB>, Xu et al., 2022)

526

527 ***Author contributions***

528 MX designed the research. ZX, WF, YW, and HY performed laboratory experiments.

529 ZX, WF, and MX analyzed the data. ZX and MX wrote the paper with significant

530 contributions from YW and HL.

531

532 ***Competing interests***

533 The authors declare that they have no conflict of interest.

534

535 ***Acknowledgments***

536 This work was supported by the National Natural Science Foundation of China

537 (NSFC, 42177211, 41701551).

538

539 **References**

540 Al-Abadleh, H. A.: Aging of atmospheric aerosols and the role of iron in catalyzing brown carbon
541 formation, *Environ. Sci.: Atmos.*, 1, 297-345, 10.1039/D1EA00038A, 2021.

542 Atwi, K., Cheng, Z., El Hajj, O., Perrie, C., and Saleh, R.: A dominant contribution to light absorption
543 by methanol-insoluble brown carbon produced in the combustion of biomass fuels typically
544 consumed in wildland fires in the United States, *Environ. Sci.: Atmos.*, 10.1039/D1EA00065A, 2022.

545 Bai, Z., Zhang, L., Cheng, Y., Zhang, W., Mao, J., Chen, H., Li, L., Wang, L., and Chen, J.:
546 Water/methanol-insoluble brown carbon can dominate aerosol-enhanced light absorption in port
547 cities, *Environ. Sci. Technol.*, 54, 14889-14898, 10.1021/acs.est.0c03844, 2020.

548 Chen, Y., and Bond, T. C.: Light absorption by organic carbon from wood combustion, *Atmos. Chem.*
549 *Phys.*, 10, 1773-1787, 10.5194/acp-10-1773-2010, 2010.

550 Cheng, Z., Atwi, K., Hajj, O. E., Ijeli, I., Fischer, D. A., Smith, G., and Saleh, R.: Discrepancies between
551 brown carbon light-absorption properties retrieved from online and offline measurements, *Aerosol*
552 *Sci. Technol.*, 55, 92-103, 10.1080/02786826.2020.1820940, 2021.

553 Chin, H., Hopstock, K. S., Fleming, L. T., Nizkorodov, S. A., and Al-Abadleh, H. A.: Effect of aromatic
554 ring substituents on the ability of catechol to produce brown carbon in iron(iii)-catalyzed reactions,
555 *Environ. Sci.: Atmos.*, 1, 64-78, 10.1039/D0EA00007H, 2021.

556 Dall'Osto, M., Querol, X., Amato, F., Karanasiou, A., Lucarelli, F., Nava, S., Calzolari, G., and Chiari,
557 M.: Hourly elemental concentrations in PM_{2.5} aerosols sampled simultaneously at urban
558 background and road site during SAPUSS – diurnal variations and PMF receptor modelling, *Atmos.*
559 *Chem. Phys.*, 13, 4375-4392, 10.5194/acp-13-4375-2013, 2013.

560 Di Lorenzo, R. A., and Young, C. J.: Size separation method for absorption characterization in brown
561 carbon: Application to an aged biomass burning sample, *Geophys. Res. Lett.*, 43, 458-465,
562 10.1002/2015gl066954, 2016.

563 Di Lorenzo, R. A., Washenfelder, R. A., Attwood, A. R., Guo, H., Xu, L., Ng, N. L., Weber, R. J.,
564 Baumann, K., Edgerton, E., and Young, C. J.: Molecular-size-separated brown carbon absorption for

565 biomass-burning aerosol at multiple field sites, *Environ. Sci. Technol.*, 51, 3128-3137,
566 10.1021/acs.est.6b06160, 2017.

567 Du, Z., He, K., Cheng, Y., Duan, F., Ma, Y., Liu, J., Zhang, X., Zheng, M., and Weber, R.: A yearlong
568 study of water-soluble organic carbon in Beijing I: Sources and its primary vs. secondary nature,
569 *Atmos. Environ.*, 92, 514-521, <https://doi.org/10.1016/j.atmosenv.2014.04.060>, 2014.

570 Feng, Y., Ramanathan, V., and Kotamarthi, V. R.: Brown carbon: a significant atmospheric absorber of
571 solar radiation? *Atmos. Chem. Phys.*, 13, 8607-8621, 10.5194/acp-13-8607-2013, 2013.

572 Gou, Y., Qin, C., Liao, H., and Xie, M.: Measurements, gas/particle partitioning, and sources of nonpolar
573 organic molecular markers at a suburban site in the west Yangtze River Delta, China, *J. Geophys.*
574 *Res. Atmos.*, 126, e2020JD034080, <https://doi.org/10.1029/2020JD034080>, 2021.

575 Hallar, A. G., Lowenthal, D. H., Clegg, S. L., Samburova, V., Taylor, N., Mazzoleni, L. R., Zielinska, B.
576 K., Kristensen, T. B., Chirokova, G., McCubbin, I. B., Dodson, C., and Collins, D.: Chemical and
577 hygroscopic properties of aerosol organics at Storm Peak Laboratory, *J. Geophys. Res. Atmos.*, 118,
578 4767-4779, <https://doi.org/10.1002/jgrd.50373>, 2013.

579 Hecobian, A., Zhang, X., Zheng, M., Frank, N., Edgerton, E. S., and Weber, R. J.: Water-Soluble Organic
580 Aerosol material and the light-absorption characteristics of aqueous extracts measured over the
581 Southeastern United States, *Atmos. Chem. Phys.*, 10, 5965-5977, 10.5194/acp-10-5965-2010, 2010.

582 Hems, R. F., Schnitzler, E. G., Liu-Kang, C., Cappa, C. D., and Abbatt, J. P. D.: Aging of atmospheric
583 brown carbon aerosol, *ACS Earth Space Chem.*, 5, 722-748, 10.1021/acsearthspacechem.0c00346,
584 2021.

585 Huang, R.-J., Yang, L., Cao, J., Chen, Y., Chen, Q., Li, Y., Duan, J., Zhu, C., Dai, W., Wang, K., Lin, C.,
586 Ni, H., Corbin, J. C., Wu, Y., Zhang, R., Tie, X., Hoffmann, T., O'Dowd, C., and Dusek, U.: Brown
587 carbon aerosol in urban Xi'an, northwest China: The composition and light absorption properties,
588 *Environ. Sci. Technol.*, 52, 6825-6833, 10.1021/acs.est.8b02386, 2018.

589 Huang, R.-J., Yang, L., Shen, J., Yuan, W., Gong, Y., Guo, J., Cao, W., Duan, J., Ni, H., Zhu, C., Dai, W.,
590 Li, Y., Chen, Y., Chen, Q., Wu, Y., Zhang, R., Dusek, U., O'Dowd, C., and Hoffmann, T.: Water-
591 insoluble organics dominate brown carbon in wintertime urban aerosol of China: Chemical
592 characteristics and optical properties, *Environ. Sci. Technol.*, 54, 7836-7847,
593 10.1021/acs.est.0c01149, 2020.

594 Hyslop, N. P., and White, W. H.: An evaluation of interagency monitoring of protected visual
595 environments (IMPROVE) collocated precision and uncertainty estimates, *Atmos. Environ.*, 42,
596 2691-2705, <https://doi.org/10.1016/j.atmosenv.2007.06.053>, 2008.

597 Kasthuriarachchi, N. Y., Rivellini, L.-H., Chen, X., Li, Y. J., and Lee, A. K. Y.: Effect of relative humidity
598 on secondary brown carbon formation in aqueous droplets, *Environ. Sci. Technol.*, 54, 13207-13216,
599 10.1021/acs.est.0c01239, 2020.

600 Kondo, Y., Miyazaki, Y., Takegawa, N., Miyakawa, T., Weber, R. J., Jimenez, J. L., Zhang, Q., and
601 Worsnop, D. R.: Oxygenated and water-soluble organic aerosols in Tokyo, *J. Geophys. Res. Atmos.*,
602 112, D01203, 10.1029/2006jd007056, 2007.

603 Lack, D. A., Langridge, J. M., Bahreini, R., Cappa, C. D., Middlebrook, A. M., and Schwarz, J. P.: Brown
604 carbon and internal mixing in biomass burning particles, *Proc. Natl. Acad. Sci. U.S.A.*, 109, 14802-
605 14807, 10.1073/pnas.1206575109, 2012.

606 Laskin, A., Laskin, J., and Nizkorodov, S. A.: Chemistry of atmospheric brown carbon, *Chem. Rev.*, 115,
607 4335-4382, 10.1021/cr5006167, 2015.

608 Li, X., Yang, Y., Liu, S., Zhao, Q., Wang, G., and Wang, Y.: Light absorption properties of brown carbon
609 (BrC) in autumn and winter in Beijing: Composition, formation and contribution of nitrated aromatic
610 compounds, *Atmos. Environ.*, 223, 117289, <https://doi.org/10.1016/j.atmosenv.2020.117289>, 2020.

611 Li, Y., Ji, Y., Zhao, J., Wang, Y., Shi, Q., Peng, J., Wang, Y., Wang, C., Zhang, F., Wang, Y., Seinfeld, J.
612 H., and Zhang, R.: Unexpected oligomerization of small α -dicarbonyls for secondary organic aerosol
613 and brown carbon formation, *Environ. Sci. Technol.*, 55, 4430-4439, 10.1021/acs.est.0c08066, 2021.

614 Lin, P., Laskin, J., Nizkorodov, S. A., and Laskin, A.: Revealing brown carbon chromophores produced
615 in reactions of methylglyoxal with ammonium sulfate, *Environ. Sci. Technol.*, 49, 14257-14266,
616 10.1021/acs.est.5b03608, 2015a

617 Lin, P., Liu, J. M., Shilling, J. E., Kathmann, S. M., Laskin, J., and Laskin, A.: Molecular characterization
618 of brown carbon (BrC) chromophores in secondary organic aerosol generated from photo-oxidation
619 of toluene, *Phys. Chem. Chem. Phys.*, 17, 23312-23325, 10.1039/c5cp02563j, 2015b.

620 Lin, P., Bluvshstein, N., Rudich, Y., Nizkorodov, S. A., Laskin, J., and Laskin, A.: Molecular chemistry of
621 atmospheric brown carbon inferred from a nationwide biomass burning event, *Environ. Sci. Technol.*,
622 51, 11561-11570, 10.1021/acs.est.7b02276, 2017.

623 Lin, P., Aiona, P. K., Li, Y., Shiraiwa, M., Laskin, J., Nizkorodov, S. A., and Laskin, A.: Molecular

624 characterization of brown carbon in biomass burning aerosol particles, *Environ. Sci. Technol.*, 50,
625 11815-11824, 10.1021/acs.est.6b03024, 2016.

626 Lin, Y.-H., Budisulistiorini, S. H., Chu, K., Siejack, R. A., Zhang, H., Riva, M., Zhang, Z., Gold, A.,
627 Kautzman, K. E., and Surratt, J. D.: Light-absorbing oligomer formation in secondary organic
628 aerosol from reactive uptake of isoprene epoxydiols, *Environ. Sci. Technol.*, 48, 12012-12021,
629 10.1021/es503142b, 2014.

630 Link, N., Removski, N., Yun, J., Fleming, L. T., Nizkorodov, S. A., Bertram, A. K., and Al-Abadleh, H.
631 A.: Dust-catalyzed oxidative polymerization of catechol and its impacts on ice nucleation efficiency
632 and optical properties, *ACS Earth Space Chem.*, 4, 1127-1139, 10.1021/acsearthspacechem.0c00107,
633 2020.

634 Liu, J., Bergin, M., Guo, H., King, L., Kotra, N., Edgerton, E., and Weber, R. J.: Size-resolved
635 measurements of brown carbon in water and methanol extracts and estimates of their contribution to
636 ambient fine-particle light absorption, *Atmos. Chem. Phys.*, 13, 12389-12404, 10.5194/acp-13-
637 12389-2013, 2013.

638 Liu, J., Lin, P., Laskin, A., Laskin, J., Kathmann, S. M., Wise, M., Caylor, R., Imholt, F., Selimovic, V.,
639 and Shilling, J. E.: Optical properties and aging of light-absorbing secondary organic aerosol, *Atmos.*
640 *Chem. Phys.*, 16, 12815-12827, 10.5194/acp-16-12815-2016, 2016.

641 Lu, Z., Streets, D. G., Winijkul, E., Yan, F., Chen, Y., Bond, T. C., Feng, Y., Dubey, M. K., Liu, S., Pinto,
642 J. P., and Carmichael, G. R.: Light absorption properties and radiative effects of primary organic
643 aerosol emissions, *Environ. Sci. Technol.*, 49, 4868-4877, 10.1021/acs.est.5b00211, 2015.

644 Lukács, H., Gelencsér, A., Hammer, S., Puxbaum, H., Pio, C., Legrand, M., Kasper-Giebl, A., Handler,
645 M., Limbeck, A., Simpson, D., and Preunkert, S.: Seasonal trends and possible sources of brown
646 carbon based on 2-year aerosol measurements at six sites in Europe, *J. Geophys. Res. Atmos.*, 112,
647 <https://doi.org/10.1029/2006JD008151>, 2007.

648 Mack, L. A., Levin, E. J. T., Kreidenweis, S. M., Obrist, D., Moosmüller, H., Lewis, K. A., Arnott, W. P.,
649 McMeeking, G. R., Sullivan, A. P., Wold, C. E., Hao, W. M., Collett Jr, J. L., and Malm, W. C.:
650 Optical closure experiments for biomass smoke aerosols, *Atmos. Chem. Phys.*, 10, 9017-9026,
651 10.5194/acp-10-9017-2010, 2010.

652 Mo, Y., Li, J., Liu, J., Zhong, G., Cheng, Z., Tian, C., Chen, Y., and Zhang, G.: The influence of solvent
653 and pH on determination of the light absorption properties of water-soluble brown carbon, *Atmos.*
654 *Environ.*, 161, 90-98, <https://doi.org/10.1016/j.atmosenv.2017.04.037>, 2017.

655 Mohr, C., Lopez-Hilfiker, F. D., Zotter, P., Prévôt, A. S. H., Xu, L., Ng, N. L., Herndon, S. C., Williams,
656 L. R., Franklin, J. P., Zahniser, M. S., Worsnop, D. R., Knighton, W. B., Aiken, A. C., Gorkowski,
657 K. J., Dubey, M. K., Allan, J. D., and Thornton, J. A.: Contribution of nitrated phenols to wood
658 burning brown carbon light absorption in Detling, United Kingdom during winter time, *Environ. Sci.*
659 *Technol.*, 47, 6316-6324, 10.1021/es400683v, 2013.

660 Moschos, V., Gysel-Ber, M., Modini, R. L., Corbin, J. C., Massabò, D., Costa, C., Danelli, S. G.,
661 Vlachou, A., Daellenbach, K. R., Szidat, S., Prati, P., Prévôt, A. S. H., Baltensperger, U., and El
662 Haddad, I.: Source-specific light absorption by carbonaceous components in the complex aerosol
663 matrix from yearly filter-based measurements, *Atmos. Chem. Phys.*, 21, 12809-12833, 10.5194/acp-
664 21-12809-2021, 2021.

665 Mi, H.-H., Lee, W.-J., Chen, C.-B., Yang, H.-H., and Wu, S.-J.: Effect of fuel aromatic content on PAH
666 emission from a heavy-duty diesel engine, *Chemosphere*, 41, 1783-1790,
667 [https://doi.org/10.1016/S0045-6535\(00\)00043-6](https://doi.org/10.1016/S0045-6535(00)00043-6), 2000.

668 Nakayama, T., Matsumi, Y., Sato, K., Imamura, T., Yamazaki, A., and Uchiyama, A.: Laboratory studies
669 on optical properties of secondary organic aerosols generated during the photooxidation of toluene
670 and the ozonolysis of α -pinene, *J. Geophys. Res. Atmos.*, 115, D24204, 10.1029/2010jd014387,
671 2010.

672 Nakayama, T., Sato, K., Tsuge, M., Imamura, T., and Matsumi, Y.: Complex refractive index of secondary
673 organic aerosol generated from isoprene/NO_x photooxidation in the presence and absence of SO₂,
674 *J. Geophys. Res. Atmos.*, 120, 7777-7787, <https://doi.org/10.1002/2015JD023522>, 2015.

675 Nguyen, T. B., Lee, P. B., Updyke, K. M., Bones, D. L., Laskin, J., Laskin, A., and Nizkorodov, S. A.:
676 Formation of nitrogen- and sulfur-containing light-absorbing compounds accelerated by evaporation
677 of water from secondary organic aerosols, *J. Geophys. Res. Atmos.*, 117, D01207,
678 10.1029/2011jd016944, 2012.

679 Powelson, M. H., Espelien, B. M., Hawkins, L. N., Galloway, M. M., and De Haan, D. O.: Brown carbon
680 formation by aqueous-phase carbonyl compound reactions with amines and ammonium sulfate,
681 *Environ. Sci. Technol.*, 48, 985-993, 10.1021/es4038325, 2014.

682 Qin, C., Gou, Y., Wang, Y., Mao, Y., Liao, H., Wang, Q., and Xie, M.: Gas-particle partitioning of polyol

683 tracers at a suburban site in Nanjing, east China: increased partitioning to the particle phase, *Atmos.*
684 *Chem. Phys.*, 21, 12141-12153, 10.5194/acp-21-12141-2021, 2021.

685 Rogge, W. F., Hildemann, L. M., Mazurek, M. A., Cass, G. R., and Simoneit, B. R. T.: Sources of fine
686 organic aerosol 4. Particulate abrasion products from leaf surfaces of urban plants, *Environ. Sci.*
687 *Technol.*, 27, 2700-2711, 10.1021/es00049a008, 1993.

688 Saleh, R., Hennigan, C. J., McMeeking, G. R., Chuang, W. K., Robinson, E. S., Coe, H., Donahue, N.
689 M., and Robinson, A. L.: Absorptivity of brown carbon in fresh and photo-chemically aged biomass-
690 burning emissions, *Atmos. Chem. Phys.*, 13, 7683-7693, 10.5194/acp-13-7683-2013, 2013.

691 Saleh, R., Robinson, E. S., Tkacik, D. S., Ahern, A. T., Liu, S., Aiken, A. C., Sullivan, R. C., Presto, A.
692 A., Dubey, M. K., Yokelson, R. J., Donahue, N. M., and Robinson, A. L.: Brownness of organics in
693 aerosols from biomass burning linked to their black carbon content, *Nat. Geosci.*, 7, 647-650,
694 <https://doi.org/10.1038/ngeo2220>, 2014.

695 Saleh, R.: From measurements to models: Toward accurate representation of brown carbon in climate
696 calculations, *Curr. Pollut. Rep.*, 6, 90-104, 10.1007/s40726-020-00139-3, 2020.

697 Schauer, J. J., Mader, B. T., Deminter, J. T., Heidemann, G., Bae, M. S., Seinfeld, J. H., Flagan, R. C.,
698 Cary, R. A., Smith, D., Huebert, B. J., Bertram, T., Howell, S., Kline, J. T., Quinn, P., Bates, T.,
699 Turpin, B., Lim, H. J., Yu, J. Z., Yang, H., and Keywood, M. D.: ACE-Asia intercomparison of a
700 thermal-optical method for the determination of particle-phase organic and elemental carbon,
701 *Environ. Sci. Technol.*, 37, 993-1001, 10.1021/es020622f, 2003.

702 Shetty, N. J., Pandey, A., Baker, S., Hao, W. M., and Chakrabarty, R. K.: Measuring light absorption by
703 freshly emitted organic aerosols: Optical artifacts in traditional solvent-extraction-based methods,
704 *Atmos. Chem. Phys.*, 19, 8817-8830, 10.5194/acp-19-8817-2019, 2019.

705 Simoneit, B. R. T., and Fetzer, J. C.: High molecular weight polycyclic aromatic hydrocarbons in
706 hydrothermal petroleum from the Gulf of California and Northeast Pacific Ocean, *Org. Geochem.*,
707 24, 1065-1077, [https://doi.org/10.1016/S0146-6380\(96\)00081-2](https://doi.org/10.1016/S0146-6380(96)00081-2), 1996.

708 Simoneit, B. R. T., Elias, V. O., Kobayashi, M., Kawamura, K., Rushdi, A. I., Medeiros, P. M., Rogge,
709 W. F., and Didyk, B. M.: Sugars dominant water-soluble organic compounds in soils and
710 characterization as tracers in atmospheric particulate matter, *Environ. Sci. Technol.*, 38, 5939-5949,
711 10.1021/es0403099, 2004.

712 Song, C., Gyawali, M., Zaveri, R. A., Shilling, J. E., and Arnott, W. P.: Light absorption by secondary
713 organic aerosol from α -pinene: Effects of oxidants, seed aerosol acidity, and relative humidity, *J.*
714 *Geophys. Res. Atmos.*, 118, 11,741-711,749, 10.1002/jgrd.50767, 2013.

715 Taylor, N. F., Collins, D. R., Lowenthal, D. H., McCubbin, I. B., Hallar, A. G., Samburova, V., Zielinska,
716 B., Kumar, N., and Mazzoleni, L. R.: Hygroscopic growth of water soluble organic carbon isolated
717 from atmospheric aerosol collected at US national parks and Storm Peak Laboratory, *Atmos. Chem.*
718 *Phys.*, 17, 2555-2571, 10.5194/acp-17-2555-2017, 2017.

719 Teich, M., van Pinxteren, D., Wang, M., Kecorius, S., Wang, Z., Müller, T., Močnik, G., and Herrmann,
720 H.: Contributions of nitrated aromatic compounds to the light absorption of water-soluble and
721 particulate brown carbon in different atmospheric environments in Germany and China, *Atmos.*
722 *Chem. Phys.*, 17, 1653-1672, 10.5194/acp-17-1653-2017, 2017.

723 Updyke, K. M., Nguyen, T. B., and Nizkorodov, S. A.: Formation of brown carbon via reactions of
724 ammonia with secondary organic aerosols from biogenic and anthropogenic precursors, *Atmos.*
725 *Environ.*, 63, 22-31, <https://doi.org/10.1016/j.atmosenv.2012.09.012>, 2012.

726 Wang, X., Heald, C. L., Ridley, D. A., Schwarz, J. P., Spackman, J. R., Perring, A. E., Coe, H., Liu, D.,
727 and Clarke, A. D.: Exploiting simultaneous observational constraints on mass and absorption to
728 estimate the global direct radiative forcing of black carbon and brown carbon, *Atmos. Chem. Phys.*,
729 14, 10989-11010, 10.5194/acp-14-10989-2014, 2014.

730 Wang, X., Heald, C. L., Liu, J., Weber, R. J., Campuzano-Jost, P., Jimenez, J. L., Schwarz, J. P., and
731 Perring, A. E.: Exploring the observational constraints on the simulation of brown carbon, *Atmos.*
732 *Chem. Phys.*, 18, 635-653, 10.5194/acp-18-635-2018, 2018.

733 Wang, Y., Hu, M., Wang, Y., Zheng, J., Shang, D., Yang, Y., Liu, Y., Li, X., Tang, R., Zhu, W., Du, Z.,
734 Wu, Y., Guo, S., Wu, Z., Lou, S., Hallquist, M., and Yu, J. Z.: The formation of nitro-aromatic
735 compounds under high NO_x and anthropogenic VOC conditions in urban Beijing, China, *Atmos.*
736 *Chem. Phys.*, 19, 7649-7665, 10.5194/acp-19-7649-2019, 2019.

737 Washenfelder, R. A., Attwood, A. R., Brock, C. A., Guo, H., Xu, L., Weber, R. J., Ng, N. L., Allen, H.
738 M., Ayres, B. R., Baumann, K., Cohen, R. C., Draper, D. C., Duffey, K. C., Edgerton, E., Fry, J. L.,
739 Hu, W. W., Jimenez, J. L., Palm, B. B., Romer, P., Stone, E. A., Wooldridge, P. J., and Brown, S. S.:
740 Biomass burning dominates brown carbon absorption in the rural southeastern United States,
741 *Geophys. Res. Lett.*, 42, 653-664, 10.1002/2014gl062444, 2015.

742 Weber, R. J., Sullivan, A. P., Peltier, R. E., Russell, A., Yan, B., Zheng, M., de Gouw, J., Warneke, C.,
743 Brock, C., Holloway, J. S., Atlas, E. L., and Edgerton, E.: A study of secondary organic aerosol
744 formation in the anthropogenic-influenced southeastern United States, *J. Geophys. Res. Atmos.*, 112,
745 D13302, 10.1029/2007jd008408, 2007.

746 Xie, M., Chen, X., Hays, M. D., Lewandowski, M., Offenber, J., Kleindienst, T. E., and Holder, A. L.:
747 Light absorption of secondary organic aerosol: Composition and contribution of nitroaromatic
748 compounds, *Environ. Sci. Technol.*, 51, 11607-11616, 10.1021/acs.est.7b03263, 2017a.

749 Xie, M., Hays, M. D., and Holder, A. L.: Light-absorbing organic carbon from prescribed and laboratory
750 biomass burning and gasoline vehicle emissions, *Sci. Rep.*, 7, 7318, 10.1038/s41598-017-06981-8,
751 2017b.

752 Xie, M., Shen, G., Holder, A. L., Hays, M. D., and Jetter, J. J.: Light absorption of organic carbon emitted
753 from burning wood, charcoal, and kerosene in household cookstoves, *Environ. Pollut.*, 240, 60-67,
754 <https://doi.org/10.1016/j.envpol.2018.04.085>, 2018.

755 Xie, M., Chen, X., Hays, M. D., and Holder, A. L.: Composition and light absorption of N-containing
756 aromatic compounds in organic aerosols from laboratory biomass burning, *Atmos. Chem. Phys.*, 19,
757 2899-2915, 10.5194/acp-19-2899-2019, 2019a.

758 Xie, M., Chen, X., Holder, A. L., Hays, M. D., Lewandowski, M., Offenber, J. H., Kleindienst, T. E.,
759 Jaoui, M., and Hannigan, M. P.: Light absorption of organic carbon and its sources at a southeastern
760 U.S. location in summer, *Environ. Pollut.*, 244, 38-46, <https://doi.org/10.1016/j.envpol.2018.09.125>,
761 2019b.

762 Xie, M., Zhao, Z., Holder, A. L., Hays, M. D., Chen, X., Shen, G., Jetter, J. J., Champion, W. M., and
763 Wang, Q.: Chemical composition, structures, and light absorption of N-containing aromatic
764 compounds emitted from burning wood and charcoal in household cookstoves, *Atmos. Chem. Phys.*,
765 20, 14077-14090, 10.5194/acp-20-14077-2020, 2020.

766 Xie, M., Peng, X., Shang, Y., Yang, L., Zhang, Y., Wang, Y., and Liao, H.: Collocated measurements of
767 Light-absorbing organic carbon in PM_{2.5}: Observation uncertainty and organic tracer-based source
768 apportionment, *J. Geophys. Res. Atmos.*, 127, e2021JD035874,
769 <https://doi.org/10.1029/2021JD035874>, 2022.

770 Xu, Z., Feng, W., Wang, Y., Ye, H., Wang, Y., Liao, H., and Xie, M.: Replication Data for:
771 Underestimation of brown carbon absorption based on the methanol extraction method and its
772 impacts on source analysis, Harvard Dataverse, V2, <https://doi.org/10.7910/DVN/CGHPXB>, 2022.

773 Xu, L., Peng, Y., Ram, K., Zhang, Y., Bao, M., and Wei, J.: Investigation of the uncertainties of simulated
774 optical properties of brown carbon at two Asian sites using a modified bulk aerosol optical scheme
775 of the community atmospheric model version 5.3, *J. Geophys. Res. Atmos.*, 126, e2020JD033942,
776 <https://doi.org/10.1029/2020JD033942>, 2021.

777 Yan, F., Kang, S., Sillanpää, M., Hu, Z., Gao, S., Chen, P., Gautam, S., Reinikainen, S.-P., and Li, C.: A
778 new method for extraction of methanol-soluble brown carbon: Implications for investigation of its
779 light absorption ability, *Environ. Pollut.*, 262, 114300, <https://doi.org/10.1016/j.envpol.2020.114300>,
780 2020.

781 Yang, L., Shang, Y., Hannigan, M. P., Zhu, R., Wang, Q. g., Qin, C., and Xie, M.: Collocated speciation
782 of PM_{2.5} using tandem quartz filters in northern nanjing, China: Sampling artifacts and
783 measurement uncertainty, *Atmos. Environ.*, 246, 118066,
784 <https://doi.org/10.1016/j.atmosenv.2020.118066>, 2021.

785 Yu, Y., Ding, F., Mu, Y., Xie, M., and Wang, Q. g.: High time-resolved PM_{2.5} composition and sources
786 at an urban site in Yangtze River Delta, China after the implementation of the APPCAP,
787 *Chemosphere*, 261, 127746, <https://doi.org/10.1016/j.chemosphere.2020.127746>, 2020.

788 Zhang, A., Wang, Y., Zhang, Y., Weber, R. J., Song, Y., Ke, Z., and Zou, Y.: Modeling the global radiative
789 effect of brown carbon: a potentially larger heating source in the tropical free troposphere than black
790 carbon, *Atmos. Chem. Phys.*, 20, 1901-1920, 10.5194/acp-20-1901-2020, 2020.

791 Zhang, X., Hecobian, A., Zheng, M., Frank, N. H., and Weber, R. J.: Biomass burning impact on PM_{2.5}
792 over the southeastern US during 2007: integrating chemically speciated FRM filter measurements,
793 MODIS fire counts and PMF analysis, *Atmos. Chem. Phys.*, 10, 6839-6853, 10.5194/acp-10-6839-
794 2010, 2010.

795 Zhang, X., Lin, Y.-H., Surratt, J. D., and Weber, R. J.: Sources, composition and absorption Ångström
796 exponent of light-absorbing organic components in aerosol extracts from the Los Angeles basin,
797 *Environ. Sci. Technol.*, 47, 3685-3693, 10.1021/es305047b, 2013.

798 Zhu, C.-S., Cao, J.-J., Huang, R.-J., Shen, Z.-X., Wang, Q.-Y., and Zhang, N.-N.: Light absorption
799 properties of brown carbon over the southeastern Tibetan Plateau, *Sci. Total Environ.*, 625, 246-251,
800 <https://doi.org/10.1016/j.scitotenv.2017.12.183>, 2018.

Table 1. SEOC concentrations and extraction efficiencies (η , %) of total OC and OC fractions for different solvents.

OC prior to extractions	Water ^a	MeOH ^b	MeOH/DCM (1:1) ^b	MeOH/DCM (1:2) ^b	THF ^b	DMF ^a	
One-time extraction (N = 11)							
<i>SEOC, $\mu\text{g m}^{-3}$</i>							
Total OC	9.36 ± 2.27	6.38 ± 2.03	7.85 ± 2.40	7.08 ± 1.32	6.99 ± 1.71	6.14 ± 2.01	8.49 ± 2.52
OC1	0.66 ± 0.21	0.61 ± 0.20	0.64 ± 0.21	0.65 ± 0.20	0.64 ± 0.22	0.59 ± 0.18	0.59 ± 0.24
OC2	2.69 ± 0.55	2.20 ± 0.60	2.50 ± 0.55	2.34 ± 0.41	2.37 ± 0.46	2.09 ± 0.55	2.48 ± 0.60
OC3	3.35 ± 0.93	1.82 ± 0.80	2.48 ± 0.96	2.23 ± 0.49	2.18 ± 0.70	1.98 ± 0.93	2.86 ± 1.01
OC4	2.75 ± 0.81	1.76 ± 0.65	2.23 ± 0.84	1.86 ± 0.51	1.78 ± 0.61	1.48 ± 0.61	2.56 ± 0.87
<i>η (%)</i>							
Total OC		66.7 ± 8.58	82.3 ± 8.68	76.0 ± 7.70	74.3 ± 7.83	64.2 ± 8.08	89.0 ± 7.96
OC1		91.7 ± 4.85	96.1 ± 6.73	97.9 ± 5.02	97.4 ± 4.35	89.6 ± 9.55	88.8 ± 4.98
OC2		80.8 ± 8.11	92.7 ± 3.69	87.7 ± 5.87	88.5 ± 7.21	76.9 ± 7.62	91.4 ± 6.17
OC3		52.4 ± 11.8	73.0 ± 11.5	68.1 ± 8.64	65.2 ± 10.2	57.6 ± 12.0	84.3 ± 9.79
OC4		63.3 ± 9.13	80.3 ± 11.4	69.0 ± 9.26	64.5 ± 8.11	52.7 ± 5.86	92.8 ± 9.69
Two-time extraction (N = 10)							
<i>SEOC, $\mu\text{g m}^{-3}$</i>							
Total OC	10.9 ± 4.93	7.74 ± 4.01	9.33 ± 4.11	9.34 ± 4.19	9.11 ± 4.04	7.56 ± 3.38	10.4 ± 4.80
OC1	0.66 ± 0.47	0.62 ± 0.45	0.62 ± 0.49	0.59 ± 0.50	0.60 ± 0.51	0.59 ± 0.49	0.60 ± 0.47
OC2	2.76 ± 0.77	2.20 ± 0.59	2.60 ± 0.66	2.57 ± 0.65	2.60 ± 0.68	2.28 ± 0.53	2.69 ± 0.78
OC3	4.11 ± 2.01	2.55 ± 1.62	3.26 ± 1.62	3.37 ± 1.68	3.20 ± 1.58	2.62 ± 1.39	3.88 ± 1.95
OC4	3.36 ± 1.77	2.38 ± 1.42	2.84 ± 1.42	2.81 ± 1.47	2.71 ± 1.39	2.08 ± 1.06	3.23 ± 1.70
<i>η (%)</i>							
Total OC		69.9 ± 5.88	86.6 ± 7.86	86.2 ± 8.73	84.8 ± 7.76	70.1 ± 8.01	95.6 ± 3.67
OC1		93.6 ± 4.08	90.3 ± 13.9	82.6 ± 25.9	83.8 ± 22.4	82.9 ± 15.1	92.2 ± 13.9
OC2		80.1 ± 5.01	94.8 ± 4.20	93.6 ± 4.94	94.7 ± 2.51	83.5 ± 6.86	97.2 ± 2.12
OC3		59.0 ± 10.6	80.0 ± 10.2	82.3 ± 9.86	79.1 ± 10.6	63.9 ± 10.7	94.2 ± 4.15
OC4		69.3 ± 6.46	86.3 ± 12.0	84.3 ± 12.0	82.7 ± 13.3	62.9 ± 7.76	96.9 ± 5.18

^a Concentrations of rOC in extracted filters were measured after the baking process (100 °C, 2 h); ^b rOC was measured when extracted filters were air dried.

Table 2. Light-absorbing properties of SEOC following one-time and two-time extraction procedures.

Solvent	Water	MeOH	MeOH/DCM (1:1)	MeOH/DCM (1:2)	THF	DMF
One-time extraction						
Abs ₃₆₅ , Mm ⁻¹	5.13 ± 2.04	11.9 ± 5.83	10.3 ± 4.42	8.12 ± 3.38	5.48 ± 3.01	17.5 ± 8.05
Abs ₅₅₀ , Mm ⁻¹	0.35 ± 0.12	1.28 ± 0.87	0.97 ± 0.55	0.35 ± 0.47	0.42 ± 0.47	4.40 ± 2.34
MAE ₃₆₅ , m ² g ⁻¹ C	0.87 ± 0.19	1.46 ± 0.41	1.41 ± 0.36	1.13 ± 0.22	0.87 ± 0.25	2.02 ± 0.58
MAE ₅₅₀ , m ² g ⁻¹ C	0.062 ± 0.028	0.15 ± 0.084	0.13 ± 0.054	0.042 ± 0.52	0.059 ± 0.56	0.30 ± 0.12
Å	6.63 ± 0.49	5.44 ± 0.75	5.65 ± 0.54	6.59 ± 0.66	6.17 ± 0.69	4.52 ± 0.41
Two-time extraction						
Abs _{365,1st} , ^a Mm ⁻¹	6.64 ± 4.25	14.1 ± 7.09	14.6 ± 8.05	11.6 ± 6.78	7.17 ± 4.26	20.5 ± 10.6
Abs _{550,1st} , ^a Mm ⁻¹	0.42 ± 0.12	1.34 ± 0.70	1.34 ± 0.83	0.84 ± 0.50	0.53 ± 0.27	2.82 ± 1.44
Abs ₃₆₅ , ^b Mm ⁻¹	8.26 ± 5.21	15.5 ± 7.76	16.8 ± 8.82	14.0 ± 8.91	8.35 ± 4.81	21.9 ± 11.2
Abs ₅₅₀ , ^b Mm ⁻¹	0.50 ± 0.18	1.60 ± 0.78	1.64 ± 0.99	1.22 ± 0.98	0.69 ± 0.43	3.01 ± 1.49
MAE ₃₆₅ , m ² g ⁻¹ C	1.19 ± 0.26	1.70 ± 0.60	1.80 ± 0.52	1.50 ± 0.51	1.10 ± 0.40	2.11 ± 0.49
MAE ₅₅₀ , m ² g ⁻¹ C	0.082 ± 0.30	0.19 ± 0.11	0.17 ± 0.083	0.13 ± 0.069	0.094 ± 0.054	0.29 ± 0.075
Å	6.32 ± 0.58	5.37 ± 0.57	5.47 ± 0.67	5.57 ± 0.39	6.06 ± 0.54	4.53 ± 0.21

^a Light absorption coefficient of SEOC after the first extraction; ^b sum of SEOC absorption in 1st and 2nd extracts.

Table 3. Comparisons of light-absorbing properties of ambient PM_{2.5} extracts in DMF and MeOH derived from duplicate Q_f-Q_b data (*N* = 109).

	DMF			MeOH ^a		
	Median	Mean ± std	Range	Median	Mean ± std	Range
Abs ₃₆₅ , Mm ⁻¹	6.99	8.42 ± 5.40	1.14–30.8	5.59	6.43 ± 4.66	0.38–29.6
MAE ₃₆₅ , m ² g ⁻¹ C	1.13	1.20 ± 0.49	0.34–2.45	0.91	1.03 ± 0.58	0.089–2.49
Å	5.21	5.25 ± 0.64	3.21–6.82	6.49	6.81 ± 1.64	4.34–11.3

^a Data for MeOH extracts were obtained from Xie et al. (2022).

Figure 1

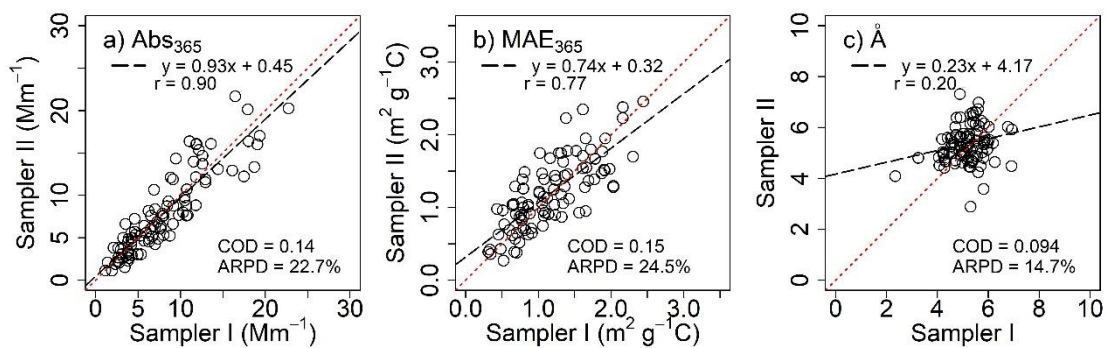


Figure 1. Comparisons between collocated measurements for light-absorbing properties of PM_{2.5} extracts in DMF after Q_b corrections.

Figure 2

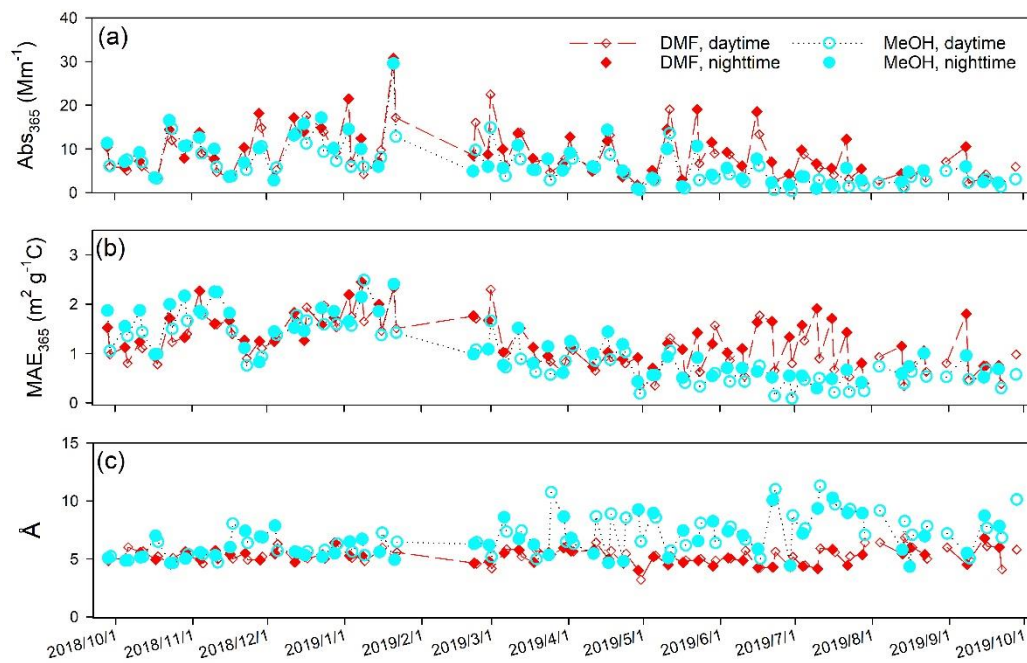


Figure 2. Time series comparisons of light-absorbing properties of DMF and MeOH extracts using artifact-corrected data. MeOH extract data were obtained from Xie et al. (2022).

Figure 3

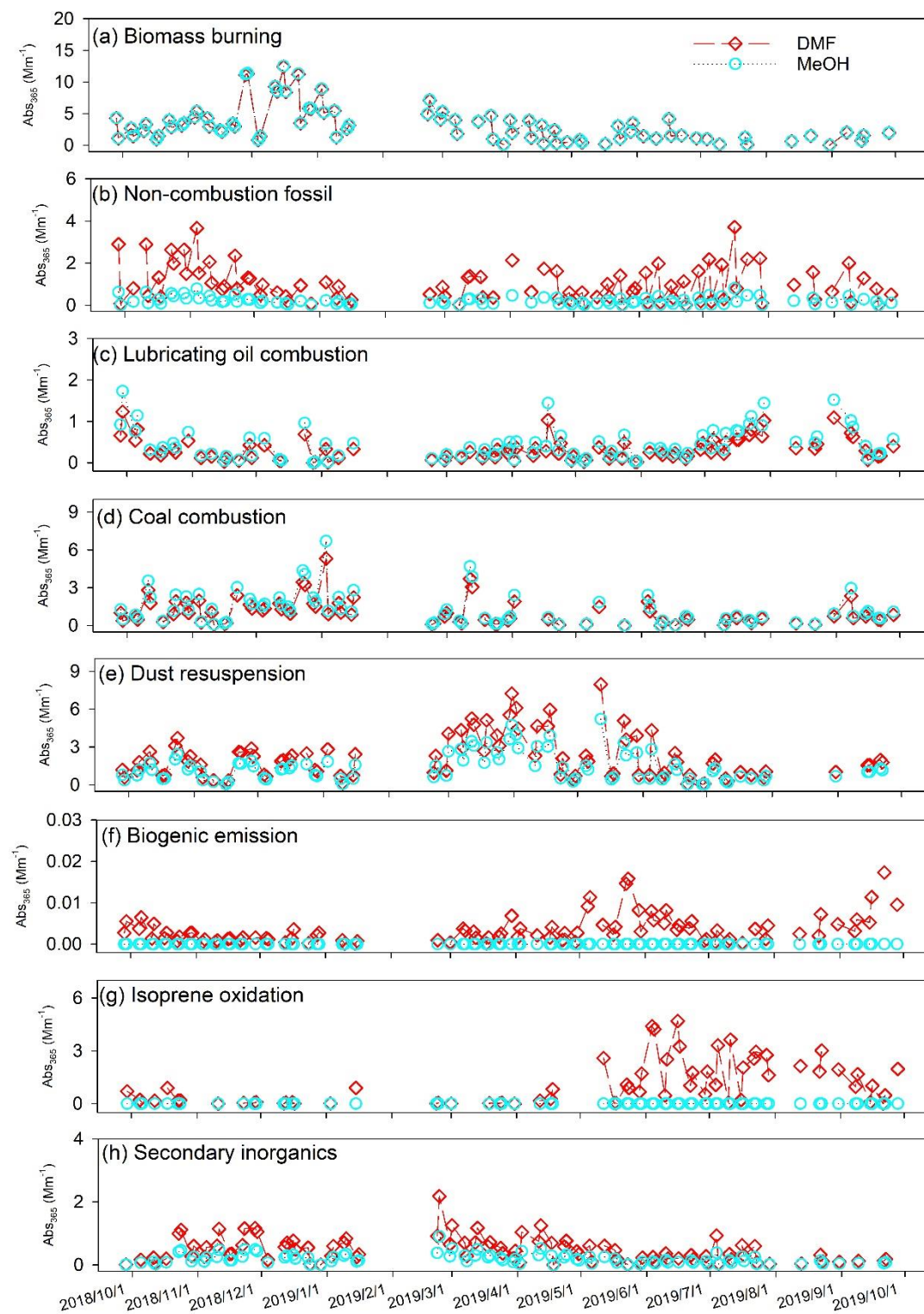


Figure 3. Time series of factor contributions to Abs_{365} of DMF and MeOH extracts of ambient PM_{2.5} samples.